

Open cluster BSS dynamical clock dependence on the Milky Way gravitational field

Andrés E. Piatti^{1,2,*}

¹Instituto Interdisciplinario de Ciencias Básicas (ICB), CONICET-UNCUYO, Padre J. Contreras 1300, M5502JMA, Mendoza, Argentina;

²Consejo Nacional de Investigaciones Científicas y Técnicas (CONICET), Godoy Cruz 2290, C1425FQB, Buenos Aires, Argentina

*Corresponding author. E-mail: andres.piatti@fcen.uncu.edu.ar

Abstract. Since recent years, mass segregation driven by two-body relaxation in star clusters has been proposed to be measured by the so-called dynamical clock, A^+ , a measure of the area enclosed between the cumulative radial distribution of blue straggler stars and that of a reference population. Since star clusters spend their lifetime immersed in the gravitational potential of their host galaxy, they are also subject to the effects of galactic tides. In this work, I show that the A^+ index of a star cluster depends on both, its internal dynamics as it were in isolation and on the effects of galactic tides. Particularly, I focused on the largest sample of open clusters harboring blue straggler stars with robust cluster membership. I found that these open clusters exhibit an overall dispersion of the A^+ index in diagnostic diagrams where Milky Way globular clusters show a clear linear trend. However, as also experienced by globular clusters, A^+ values of open clusters show some dependence on their galactocentric distances, in the sense that clusters located closer or farther than ~ 11 kpc from the Galactic center have larger and smaller A^+ values, respectively. This different response to two-body relaxation and galactic tides in globular and open clusters, which happen concurrently, can be due to their different masses. More massive clusters can somehow protect their innermost regions from galactic tides more effectively.

Keywords. Methods: data analysis — Galaxy: open clusters and associations: general

1. Introduction

It is widely accepted that mass segregation is a phenomenon observed in collisional stellar systems as one manifestation of the internal two-body relaxation process. It consists in kinematic energy exchanges between stars, which leads more massive stars to slow down and to spiral toward the innermost regions, while less massive stars increase their velocities reaching the outermost cluster regions (Alessandrini *et al.*, 2014). From a theoretical point of view, the level of mass segregation in a star cluster is given by the central relaxation time (t_{rc}), which depends on the core radius, the central mass density, the average mass of the cluster stars, and the number of cluster members (Djorgovski, 1993). In practice, the N_{relax} index is used instead, defined as the ratio between the star cluster age and t_{rc} . Because of the wide range of values of the measured parameters to compute N_{relax} , different stellar systems show different levels of mass segregation.

In a star cluster, blue straggler stars (BSSs) are in general more massive stars than Main Sequence (MS) ones; hence they have extensively been used to measure the mass segregation level of stellar systems.

They occupy a clearly identifiable region in the color-magnitude diagram at brighter magnitudes and bluer colors than the position of the MS turnoff (see, e.g. Li *et al.*, 2023). Ferraro *et al.* (2018) measured A^+ – the area enclosed between the cumulative radial distributions of BSSs and that of a reference (MS) population (see Alessandrini *et al.*, 2016) – in 27 Milky Way old globular clusters, and found that A^+ correlates with N_{relax} . From then on, A^+ has been referred to as a star cluster dynamical clock. It has been used to measure the dynamic evolutionary stage of open clusters (e.g., Rao *et al.*, 2021, 2023b). Indeed, different studies on BSSs in Milky Way open clusters have recently been published, with several updated compilations and analysis of BSS properties (Jadhav & Subramaniam, 2021; Rao *et al.*, 2023a; Rain *et al.*, 2024).

Because a star cluster moves in an external gravitational potential, tides also affect the spatial distribution of its stars and therefore the cluster structural parameters. Piatti *et al.* (2019) showed that the core, half-mass and Jacobi radii of the Milky Way globular clusters are in general larger as their galactocentric distances increase, because at larger galactocentric distances the Milky Way potential weakens, allowing the

cluster to expand. Furthermore, the pace of change with the galactocentric distance is more important for Jacobi radii than for core ones. Piatti & Mackey (2018) also studied the correlation between the cluster size and its position in its host galaxy by analyzing the population of Large Magellanic Cloud globular clusters, and found similar results. The cluster radius change caused by the host galaxy gravitational field implies that the cluster is dynamically accelerated, i.e., it is in a more advanced internal dynamics evolutionary stage in the presence of stronger tides. Consequently, tides from an external gravitational field affect the level of mass segregation in a star cluster (see also Piatti, 2020).

Open clusters are less massive than globular clusters, so that mass segregation is expected to be more affected by galactic tides. This would imply that the A^+ index needs to be corrected by tidal effects previously to be used as a cluster dynamical clock. Precisely, we analyze this phenomenon in this work. In Section 2 we describe the updated homogeneous compilation of BSSs in open clusters and the measurement of A^+ indices for robust sample of open cluster. From them, in Section 3, we analyze the dependence of A^+ with the position of the open clusters in the Milky Way, and discuss the outcomes. Section 4 summarizes the main conclusions of this work.

2. The A^+ index

Rao *et al.* (2023b, see their figure 4) analyzed 21 open clusters and showed that the correlation between A^+ and N_{relax} is moderate (0.5), with a relative wide range of internal dynamics evolutionary stages at any A^+ values, for $0.0 \leq A^+ \leq 0.2$. They arrived at this result using *Gaia* EDR3 data (*Gaia* Collaboration *et al.*, 2021) to estimate cluster properties (half-light radius, central mass density, average stellar mass, etc) from identified members. In order to probe whether such a dispersion has its origin in any dependence of the A^+ index on the effects of tides caused by the Milky Way gravitational potential, we decided to use the updated catalog of populations of BSSs in open clusters compiled by Rain *et al.* (2021). The catalog is the result of an homogeneous search for BSSs using *Gaia* photometry, proper motions, and parallaxes, along with solid assessments on their cluster membership. They used the membership probabilities obtained by Cantat-Gaudin *et al.* (2020) from *Gaia* DR2 dat sets. The stringent criteria applied allowed Rain *et al.* (2021) to identify 897 BSSs in 408 open clusters. Because most of the clusters contain very few number of BSSs, they concluded that open clusters are not a preferable environment for these kinds of stars.

From their catalog, we retrieved R.A. and Dec. coordinates, G magnitude and $BP - RB$ color, and membership probability (P (%)) for every BSS with $P > 70\%$. We used this frequently employed membership cut in star cluster photometric studies as a compromise between minimizing field contamination (e.g. $P < 50\%$) and maximizing the presence of highly ranked cluster members (e.g., $P > 90\%$). Nevertheless, in the subsequent analysis we compare the results by using stars with $P > 70\%$ and $P > 90\%$. With the aim of assuring also a reliable cluster statistics, we kept clusters with a number of BSSs inside their half member radius (r_{50} ; Cantat-Gaudin *et al.*, 2020) larger than 5, and compiled a cluster sample as large as possible (see Table 1). In the subsequent analysis, it is shown that this lower limit does not affect the results. We found a total of 18 open clusters that comply with such a requirement. We also retrieved R.A. and Dec. coordinates, G , BP , RP photometry, and membership probabilities P for stars with $P > 70\%$ from the catalog compiled by Cantat-Gaudin *et al.* (2020) of stars belonging to a reference cluster stellar population for these 18 open clusters (see below). We note that both the data sets and the membership probabilities of the BSS and reference population stars come from the same source, namely *Gaia* DR2 and the Cantat-Gaudin *et al.* (2020)'s membership assessment. We then followed the recipe outlined by Ferraro *et al.* (2018) to compute A^+ , namely: i) to build the cumulative spatial distribution function of BSSs distributed within a circular area of radius equals to the cluster half member radius; ii) to construct the corresponding cumulative spatial distribution function of a reference cluster stellar population; and iii) to compute the value of the area enclosed between both cumulative spatial distribution functions. For the calculation of the A^+ index and the subsequent analysis, we adopted the cluster central coordinates and cluster half member radii given by Cantat-Gaudin *et al.* (2020) (see Table 1).

In practice, we first matched the Cantat-Gaudin *et al.* (2020) and Rain *et al.* (2021) catalogs, and for each matched cluster we computed the distance to the cluster center of every star with $P > 70\%$, and kept those located inside r_{50} . Then, we sought for the faintest cluster BSS and used the corresponding G magnitude to define the reference population, which consisted of cluster MS stars located inside r_{50} and with G magnitudes down to 1 mag fainter than the faintest BSS G mag. This criterion allows to maximize the use of the largest number of BSSs, which can be unevenly distributed along the G magnitude when comparing one cluster to another, and thus more physically meaningfully to define the sample of reference population stars as those stars less massive than the least massive BSS

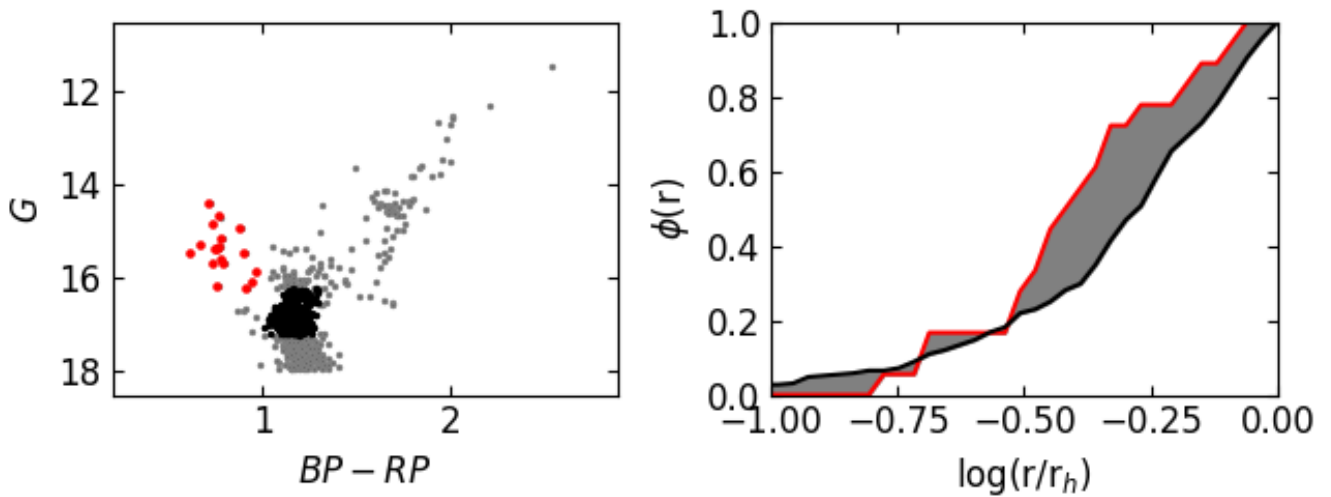


Figure 1. Left panel: *Gaia* color-magnitude diagram of NGC 2158 (gray points) for stars located inside r_{50} . Red and black points represent cluster BSSs and reference population stars with $P > 70\%$, respectively, located inside r_{50} . **Right panel:** cumulative spatial distribution function of BSSs and reference population stars drawn with red and black lines, respectively. The gray area enclosed by them represents the A^+ index.

star. We found that using a G mag interval of 0.5 mag does not imply changes in the A^+ trend with respect to different cluster properties. We applied this criterion to define the reference population of the 18 selected open clusters. We verified that the faintest MS stars used are brighter than $G \sim 18.0$ mag. Figure 1 illustrates for NGC 2158 the placement of BSSs and MS stars belonging to the reference population, highlighted with red and black points, respectively. Similar plots for the whole cluster sample are included in the Appendix.

We cumulatively added the stars using their distances to the cluster centers (r) as a variable and built the respective distribution function $\phi(r)$ in terms of $\log(r/r_{50})$, where r_{50} is the half member radius. The right panel of Figure 1 illustrates, as an example, the construction of the cumulative spatial distribution functions for BSSs and reference MS stars of NGC 2158 (see also the cumulative functions for the whole cluster sample in the Appendix). As can be seen, BSSs in NGC 2158 are more centrally concentrated than reference MS stars. The area embraced by these curves represents A^+ , which we obtained by calculating the difference between the integrals of both curves. By definition, the larger the A^+ value, the more advanced level of cluster mass segregation. Figure 2 shows that we equally employed relatively smaller and larger numbers of BSSs and r_{50} to compute A^+ , which secures our analysis against any bias in the A^+ calculation procedure. The different number of BSSs used (from 5 up to 39) is represented with filled circles of different sizes. The uncertainties in the computed A^+ values were estimated assuming that the main source of dispersion in

the A^+ values is the number of BSSs and reference MS stars used. Therefore, we repeated 20 times the procedure of computing A^+ , by considering numbers of stars whose membership probabilities randomly vary from 70% up to 90%, and adopted the largest difference between the obtained A^+ value and that for $P > 70\%$ as the uncertainty in A^+ ($\sigma(A^+)$). Table 1 lists the resulting A^+ values with their associated errors and relevant cluster properties used in this work. A comparison of the present A^+ values and those derived by Rao *et al.* (2023b) for open clusters in common is shown in Figure 24. Rao *et al.* (2023b) also computed N_{relax} for their smaller cluster sample. Computing N_{relax} is not a straightforward task, because it depends on the knowledge of the mean cluster mass, the central cluster stellar density, and the cluster core radius, which can be reliably estimated from photometric data corrected for incompleteness. Being this not the case for our entire cluster sample, nor that of Rao *et al.* (2023b) photometry (see also differences with Rao *et al.* (2021)), we preferred to conduct the subsequent analysis using widely used cluster structural parameters (Kharchenko *et al.*, 2013).

3. Analysis and discussion

We started our analysis by building Figure 3, which depicts the correlation between the core radius (r_c) derived by Kharchenko *et al.* (2013) and our resulting A^+ values for the 18 studied open clusters. Both quantities were obtained independently one to each other

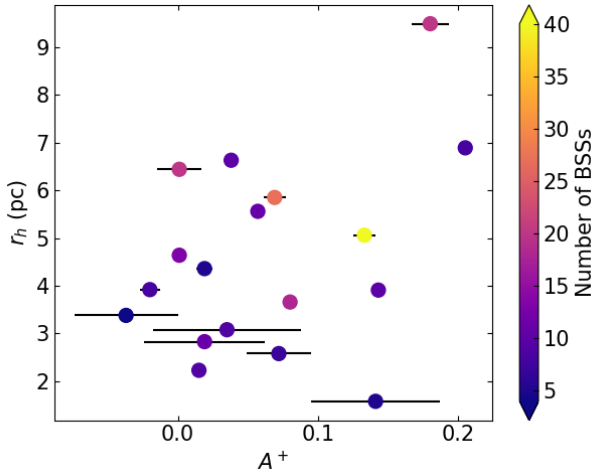


Figure 2. Relationship between the A^+ index and r_{50} for the studied cluster sample. Error bars are indicated.

and from homogeneous procedures. For the sake of the reader, we draw the relationship between both parameters and its standard deviation derived for Milky Way globular clusters by Ferraro *et al.* (2018). They also showed that N_{relax} correlates with A^+ , which we do not examine in this work because only some few open clusters have reliable N_{relax} estimates. We should expect that A^+ values of open clusters follow the linear curve drawn in Figure 3, if A^+ results in an indicator of the level of the cluster mass segregation driven by two-body relaxation as the cluster were in isolation. As can be seen, the studied open cluster sample shows an important dispersion around the fitted relationship. With the aim of disentangling the origin of such a dispersion, we colored the points according to the respective cluster galactocentric distance. At first glance, farther open clusters tend to have smaller A^+ values in comparison with those of open clusters closer to the Galactic center. Figure 4 shows the behavior of the dynamical profile of a cluster given by the concentration parameter $c = \log(r_t/r_c)$, where r_t is the tidal radius derived by Kharchenko *et al.* (2013), from which is also seen the lack of correlation with the A^+ index.

Based on Figures 3 and 4, we examined the correlation between the present A^+ values with the galactocentric distance (R_{GC}) and the maximum height above the Galactic plane (Z_{max} ; Tarricq *et al.*, 2021) for the studied cluster sample. Figure 5 shows the resulting relationship, which reveals that the A^+ index is prone to variation of the galactocentric distance, in the sense that the larger the galactocentric distance, the smaller the A^+ index. In the case of the maximum height above the Galactic plane some trend is also glimpsed, although it depends on R_{GC} , namely: for large Z values (and large R_{GC} ones) A^+ values are generally smaller than those

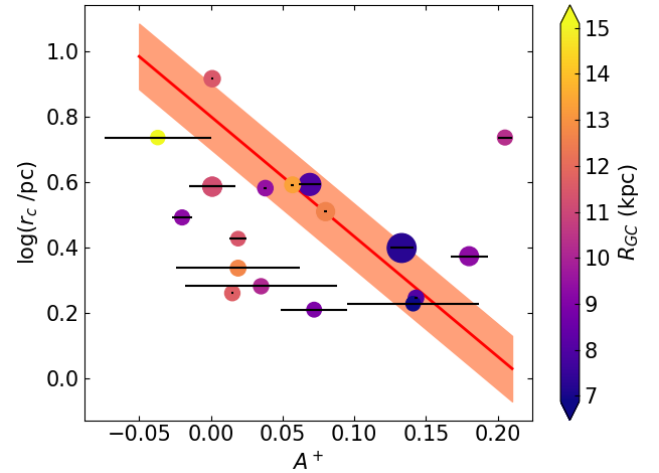


Figure 3. Relationship between the A^+ index and r_c for the studied cluster sample. Error bars are indicated. The size of the circles is proportional to the number of BSSs used to compute A^+ . The solid line and shaded region represent the fitted relationship and its uncertainty found by Ferraro *et al.* (2018) for the Milky Way globular cluster population. Pearson, Spearman, and p-value (T-test) are -0.12 , -0.12 , and 3×10^{-15} , respectively.

for smaller Z values (and smaller R_{GC} ones). The observational trend supports the idea that the Milky Way galactic potential causes –through the effects of tides– that open clusters closer to the Galactic center have larger A^+ values in comparison with their counterparts located farther from the Galactic center; mass segregation as measured by r_c and by the concentration parameter c showing an overall dispersion. This result would seem to suggest that the A^+ index for open clusters is one of the primary drivers of the effects of galactic tides rather than by r_c and c , which according to Ferraro *et al.* (2018) is sensitive to mass segregation in Milky Way globular clusters. As far as we are aware, our outcome is based on the largest sample of open clusters with A^+ index derived homogeneously. Particularly, we emphasize on the solid assessments of BSS and reference MS cluster star membership (Rain *et al.*, 2021).

Because A^+ values decrease with increasing galactocentric distances, as also the effects of galactic tides do, we draw the conclusion – although from a limited sample of 4 open clusters with $12 < R_{GC}$ (kpc) < 15 – that typical A^+ value of open clusters in the presence of a relative light external galactic field (or the absence thereof) is $\sim 0.0 \pm 0.05$ (see Figure 5). This range ($\Delta A^+ = 0.05$) is nearly 10 times smaller than that found for Milky Way globular clusters, many of them populating the Galactic halo (Ferraro *et al.*, 2018), which suggests that the A^+ index for the globular and open cluster populations behaves differently. From this specu-

lation, larger A^+ values in open clusters would come from the effect of the galactic tides, thus mimicing the more advanced mass segregation level of an open cluster dynamically evolving in isolation. Note, however, that reliable N_{relax} values are needed in order to probe whether for a given N_{relax} value, the A^+ index clearly decreases with R_{GC} . Nevertheless, if an attempt of a linear relationship between A^+ , R_{GC} , and Z_{max} were suggested, as:

$$A^+ = a_1 + a_2 \times R_{GC} + a_3 \times Z \quad (1)$$

we would obtain $a_1 = 0.244 \pm 0.069$, $a_2 = -0.019 \pm 0.006$, and $a_3 = 0.030 \pm 0.038$, with $\chi^2 = 0.004$.

We explored the different spatial distributions of BSSs and MS reference stars in open clusters with smaller and larger A^+ values using numerical simulations. We adopted a King's (King, 1962) profile to describe the stellar density distribution and played with different combinations of r_c and r_t values. We built the cumulative distribution function as described in Section 2. The values of r_c and r_t used for the reference MS stars are those coming from the average of core and tidal radii homogeneously derived for 2006 open clusters by Kharchenko *et al.* (2013). We found that mean core and tidal radii increase from ~ 0.8 pc up to 3.0 pc and from ~ 9.0 up to 50.0 pc, respectively, for R_{GC} between 7 kpc and 16 kpc. As can be seen, open clusters show a trend of increasing radii with the galactocentric distance, similarly to Large Magellanic Cloud and Milky Way globular clusters (Piatti & Mackey, 2018; Piatti *et al.*, 2019). Furthermore, the r_t/r_c ratio also increases with increasing galactocentric distances.

Figure 5 shows that outer open clusters have $A^+ \sim 0.0$. This implies that BSSs and MS reference stars are spatially distributed similarly, and hence both populations can be modeled with the same r_c and r_t values corresponding to large galactocentric distances. Figure 6 (top panel) shows the expected resulting cumulative distribution functions. In order to get $A^+ \sim 0.15$ for inner galactic disk open clusters ($R_{GC} = 7$ kpc, see Figure 5), we used the r_c and r_t values mentioned above for the MS reference stars, while for BSSs we used $r_c = 0.3$ pc and $(r_t/r_c)_{BSS} = (r_t/r_c)_{MS} = 3.75$. Figure 6 (bottom panel) depicts the two different cumulative distribution functions. Here, $r_c(BSS)$ plays an important role. We obtained similar A^+ values using $r_t(BSS)$ as large as $r_t(MS)$. However, larger $r_c(BSS)$ values lead to A^+ ones smaller than 0.15. The above simulations show that the core radius of the MS reference stars is ~ 2.7 times larger than that of the BSSs to produce $A^+ = 0.15$.

When dealing with Milky Way globular clusters, the difference between the core radii of the BSSs and MS reference stars, which implies mass segregation, is

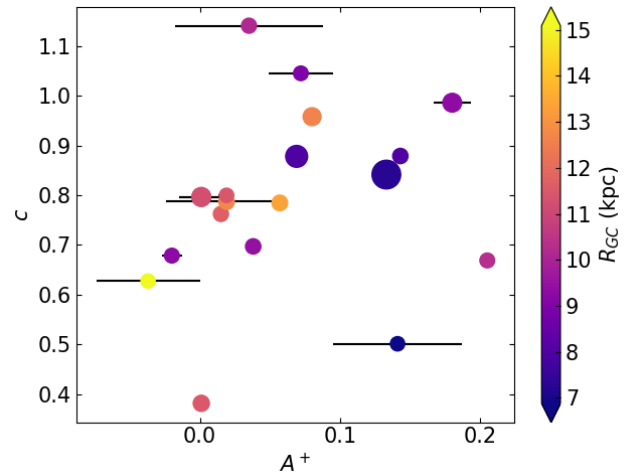


Figure 4. Relationship between the A^+ index and the concentration parameter c for the studied cluster sample. Error bars are indicated. The size of the circles is proportional to the number of BSSs used to compute A^+ . Pearson, Spearman, and p-value (T-test) are 0.06, 0.11, and 9×10^{-133} , respectively.

a function of the cluster core radius (see straight line in Figure 3). The smaller the cluster core radius, the larger the level of mass segregation (larger A^+ values). At the same time, globular cluster core radii vary with the galactocentric distance as shown by (Piatti *et al.*, 2019), adding a residual behavior of A^+ as a function of the galactocentric distance (see eq. (2) of Piatti, 2020). Here, Figure 3 shows that the A^+ index of open clusters does not directly depends on r_c . However, open clusters can exhibit some level of mass segregation, i.e., different spatial distributions of BSSs and MS reference stars, when comparing those located closer and farther than ~ 11 kpc from the Galactic center (see Figure 5). This trend suggests that the galactic tides are stronger drivers of mass segregation in open clusters than the two-body relaxation process.

4. Conclusions

It has been widely accepted that two-body relaxation led collisional systems to experience mass segregation. Recently, the A^+ index was introduced with the aim of providing a direct measure of the level of mass segregation of Milky Way globular clusters. Since then, A^+ was called a dynamical clock. However, star clusters usually are found immersed in the gravitational potential of their host galaxies, so that they are also subject of galactic tide effects. One of the manifestations of the galactic gravitation forces acting on star clusters are the observed tidal tails.

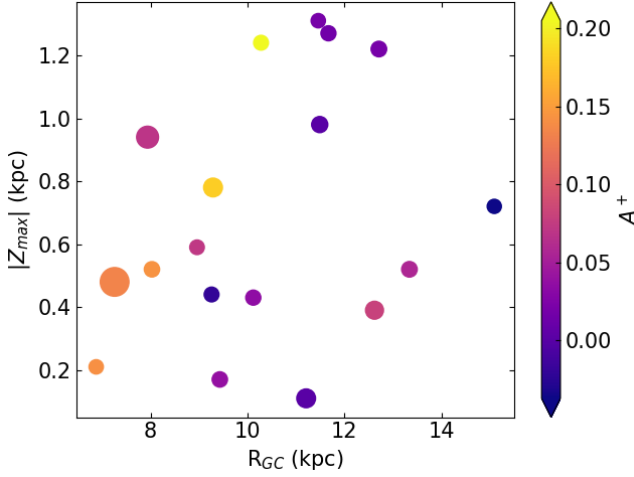


Figure 5. Relationship between the galactocentric distance (R_{GC}) and the maximum height above the Galactic plane (Z_{max}) for the studied cluster sample. The size of the circles is proportional to the number of BSSs used to compute A^+ .

Based on this evidence, an avoidable question arises: at what level the star cluster stellar density distribution is affected by galactic tides? In order to contribute to its answer, we embarked in the analysis of Milky Way and Large Magellanic Cloud globular and open clusters by examining the dependence of the A^+ index on the galactocentric distance. We found that A^+ values of globular clusters depend on both the level of two-body relaxation and their position in the galaxy (Piatti, 2020). In this present work, we analyzed the behavior of the A^+ index for a sample of Milky Way open clusters.

We used a recent updated catalog of BSSs in open clusters (Rain *et al.*, 2021) with robust assessments on their cluster membership. The final list of selected clusters contains 18 objects with more than 5 BSSs with membership probabilities $> 70\%$ and *Gaia* photometry; same requirements were fulfilled for cluster MS stars used as a reference stellar population. The derived A^+ values lead to conclude that open clusters do not show the trend with r_c shown for globular clusters, but an overall dispersion. Nevertheless, more open clusters are needed to be analyzed in order to make more definitive statements on this behavior. However, the residual correlation of the A^+ index with the cluster position in the galaxy seen for globular clusters is also apparent in the studied open cluster sample. We think that the different observed response of star clusters' internal dynamics to two-body relaxation and to galactic tides is related to their masses. More massive clusters (globular versus open clusters) can somehow protect their innermost regions from galactic tides more effectively.

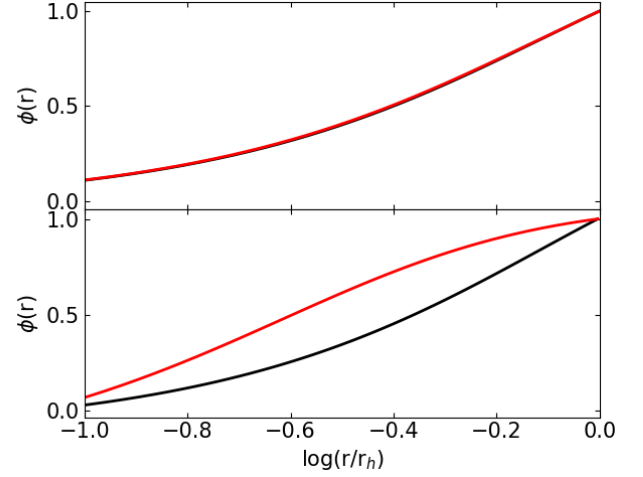


Figure 6. Cumulative distribution functions of synthetic BSS and MS reference stars drawn with red and black lines, respectively. Top and bottom panels correspond to similar and different density distributions of BSS and MS reference stars, respectively (see text for details).

Acknowledgements

We thank the referee for the thorough reading of the manuscript and timely suggestions to improve it.

Data for reproducing the figures and analysis in this work will be available upon request to the author.

References

- Alessandrini, E., Lanzoni, B., Ferraro, F. R., Miocchi, P., & Vesperini, E. 2016, *The Astrophysical Journal*, 833, 252
- Alessandrini, E., Lanzoni, B., Miocchi, P., Ciotti, L., & Ferraro, F. R. 2014, *The Astrophysical Journal*, 795, 169
- Cantat-Gaudin, T., Anders, F., Castro-Ginard, A., *et al.* 2020, *Astronomy & Astrophysics*, 640, A1
- Djorgovski, S. 1993, in *Astronomical Society of the Pacific Conference Series*, Vol. 50, *Structure and Dynamics of Globular Clusters*, ed. S. G. Djorgovski & G. Meylan, 373
- Ferraro, F. R., Lanzoni, B., Raso, S., *et al.* 2018, *The Astrophysical Journal*, 860, 36
- Gaia Collaboration, Brown, A. G. A., Vallenari, A., *et al.* 2021, *Astronomy & Astrophysics*, 649, A1
- Jadhav, V. V., & Subramaniam, A. 2021, *Monthly Notices of the Royal Astronomical Society*, 507, 1699

Table 1. A^+ estimates and astrophysical parameters for the studied cluster sample. N_{BSS} and N_{ref} refer to the number of BBS and reference stars with $P > 70\%$ located inside r_{50} , respectively.

Cluster	R.A. (deg)	Dec. (deg)	$\log(t/\text{yr})$	r_c (pc)	r_{50} (pc)	r_t (pc)	R_{GC} (kpc)	Z	A^+	N_{BSS}	N_{ref}
Berkeley 17	80.130	30.574	10.00	1.82	2.23	10.53	11.67	-0.21	0.015±0.005	9	81
Berkeley 31	104.406	8.285	9.31	5.44	3.38	23.07	15.09	0.64	-0.037±0.037	5	18
Berkeley 39	116.702	-4.665	9.90	8.23	4.64	19.81	11.49	0.69	0.001±0.004	13	123
Berkeley 99	350.260	71.778	9.50	2.67	4.36	16.84	11.46	0.90	0.019±0.006	5	19
Collinder 261	189.519	-68.377	9.95	2.50	5.06	17.36	7.26	-0.28	0.133±0.010	40	467
King 11	356.912	68.636	9.04	1.91	3.08	26.43	10.12	0.35	0.035±0.053	9	76
Melotte 66	111.573	-47.685	9.53	5.44	6.89	25.38	10.28	-1.19	0.205±0.005	8	227
NGC 188	11.798	85.244	9.88	2.36	9.49	22.86	9.28	0.65	0.180±0.014	20	222
NGC 1193	46.486	44.383	9.70	2.17	2.83	13.29	12.70	-1.05	0.019±0.043	11	60
NGC 2141	90.734	10.451	9.23	3.90	5.56	23.75	13.34	-0.52	0.057±0.003	11	156
NGC 2158	91.862	24.099	9.02	3.23	3.66	29.33	12.62	0.13	0.080±0.002	18	298
NGC 2682	132.846	11.814	9.45	1.62	2.58	17.98	8.96	0.47	0.072±0.023	7	75
NGC 6253	254.778	-52.712	9.70	1.69	1.58	5.36	6.88	-0.18	0.141±0.046	5	51
NGC 6791	290.221	37.778	9.92	3.91	5.85	29.54	7.94	0.80	0.069±0.008	27	533
NGC 6819	295.327	40.190	9.36	1.76	3.91	13.32	8.03	0.41	0.143±0.005	10	227
NGC 7142	326.290	65.782	9.55	3.10	3.92	14.79	9.25	0.40	-0.020±0.007	8	91
NGC 7789	359.334	56.726	9.52	3.81	6.63	18.87	9.43	-0.20	0.038±0.004	10	376
Trumpler 5	99.126	9.465	9.60	3.85	6.44	24.10	11.21	0.05	0.001±0.016	20	525

Kharchenko, N. V., Piskunov, A. E., Schilbach, E., Röser, S., & Scholz, R. D. 2013, *Astronomy & Astrophysics*, 558, A53

King, I. 1962, *The Astronomical Journal*, 67, 471

Li, C., Zhong, J., Qin, S., & Chen, L. 2023, *Astronomy & Astrophysics*, 672, A81

Piatti, A. E. 2020, *Research Notes of the American Astronomical Society*, 4, 248

Piatti, A. E., & Mackey, A. D. 2018, *Monthly Notices of the Royal Astronomical Society*, 478, 2164

Piatti, A. E., Webb, J. J., & Carlberg, R. G. 2019, *Monthly Notices of the Royal Astronomical Society*, 489, 4367

Rain, M. J., Ahumada, J. A., & Carraro, G. 2021, *Astronomy & Astrophysics*, 650, A67

Rain, M. J., Pera, M. S., Perren, G., *et al.* 2024, arXiv e-prints, arXiv:2402.14990

Rao, K. K., Bhattacharya, S., Vaidya, K., & Agarwal, M. 2023a, *Monthly Notices of the Royal Astronomical Society*, 518, L7

Rao, K. K., Vaidya, K., Agarwal, M., Balan, S., & Bhattacharya, S. 2023b, *Monthly Notices of the Royal Astronomical Society*, 526, 1057

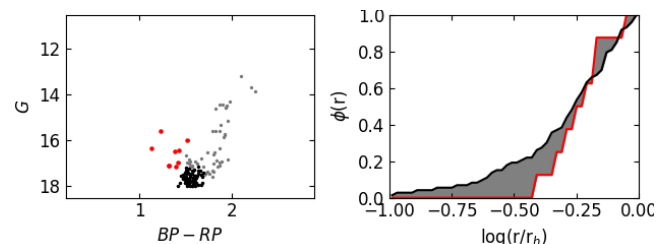


Figure 7. Same as Figure 1 for Berkeley 17.

Rao, K. K., Vaidya, K., Agarwal, M., & Bhattacharya, S. 2021, *Monthly Notices of the Royal Astronomical Society*, 508, 4919

Tarricq, Y., Soubiran, C., Casamiquela, L., *et al.* 2021, *Astronomy & Astrophysics*, 647, A19

Appendix A. The A^+ index

In this section, we present color-magnitude diagrams and cumulative distribution functions of the complete cluster sample. The figures depicts the features illustrated in Figure 1 (Section 2).

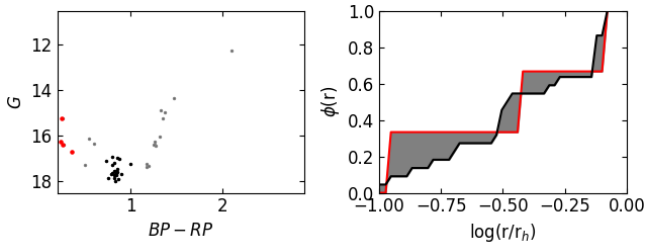


Figure 8. Same as Figure 1 for Berkeley 31.

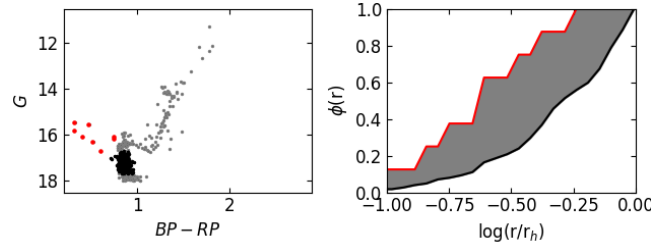


Figure 13. Same as Figure 1 for Melotte 66.

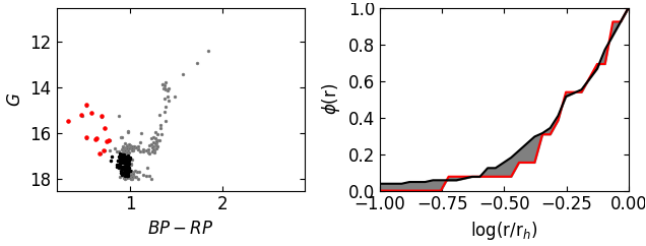


Figure 9. Same as Figure 1 for Berkeley 39.

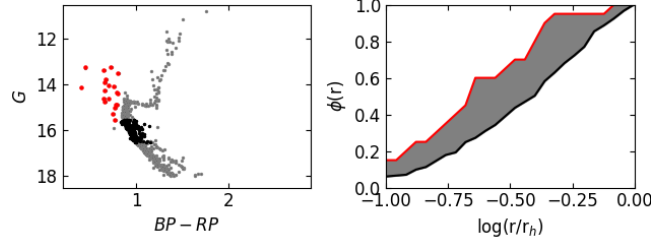


Figure 14. Same as Figure 1 for NGC 188.

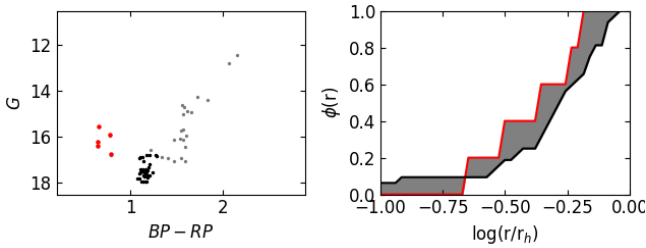


Figure 10. Same as Figure 1 for Berkeley 99.

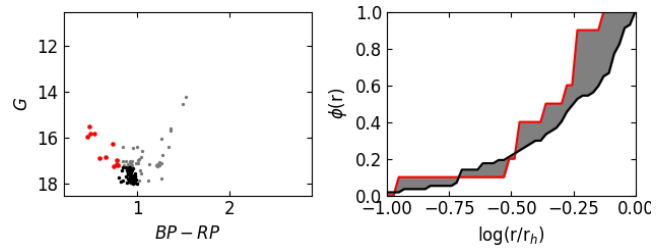


Figure 15. Same as Figure 1 for NGC 1193.

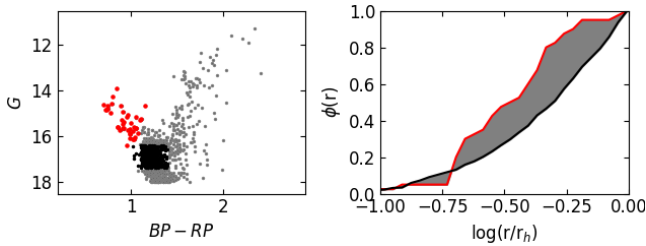


Figure 11. Same as Figure 1 for Collinder 261.

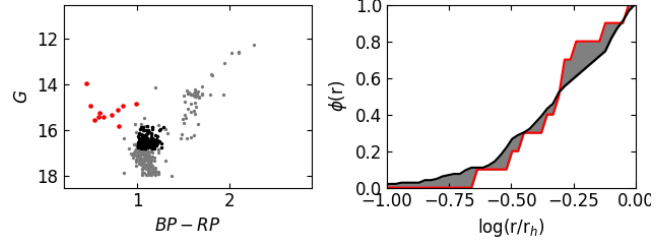


Figure 16. Same as Figure 1 for NGC 2141.

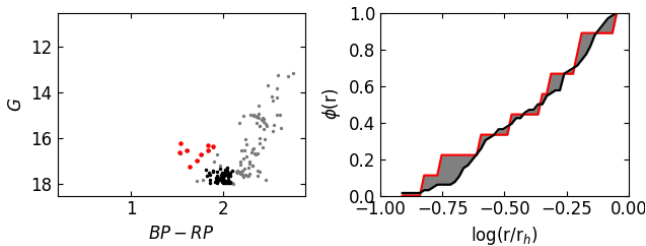


Figure 12. Same as Figure 1 for King 11.

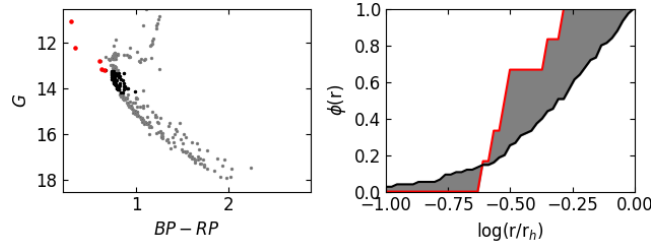


Figure 17. Same as Figure 1 for NGC 2682.

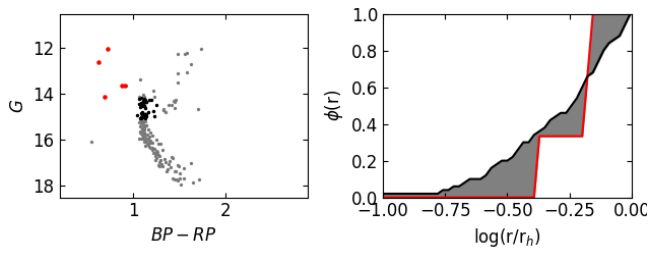


Figure 18. Same as Figure 1 for NGC 6253.

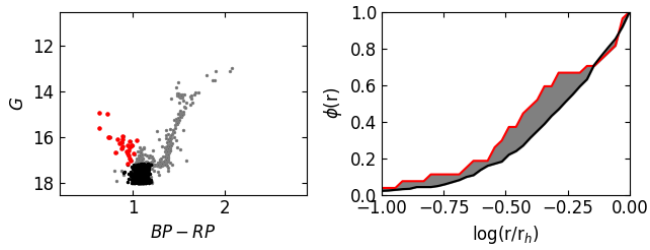


Figure 19. Same as Figure 1 for NGC 6791.

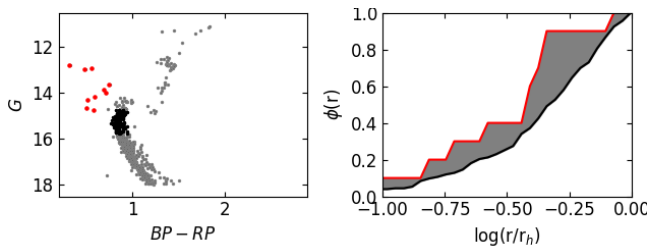


Figure 20. Same as Figure 1 for NGC 6819.

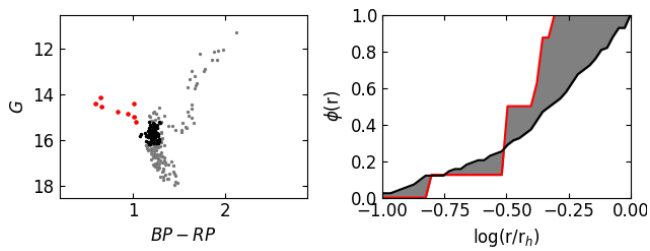


Figure 21. Same as Figure 1 for NGC 7142.

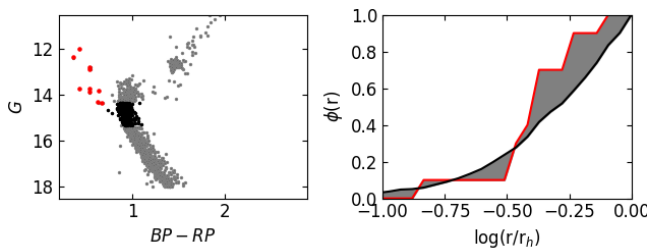


Figure 22. Same as Figure 1 for NGC 7789.

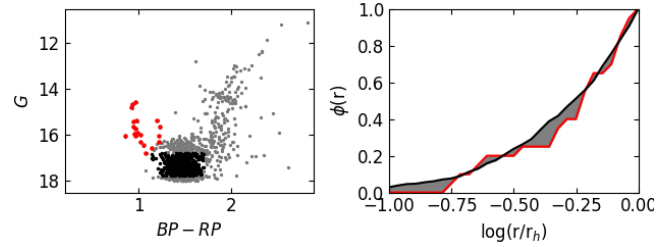


Figure 23. Same as Figure 1 for Trumpler 5.

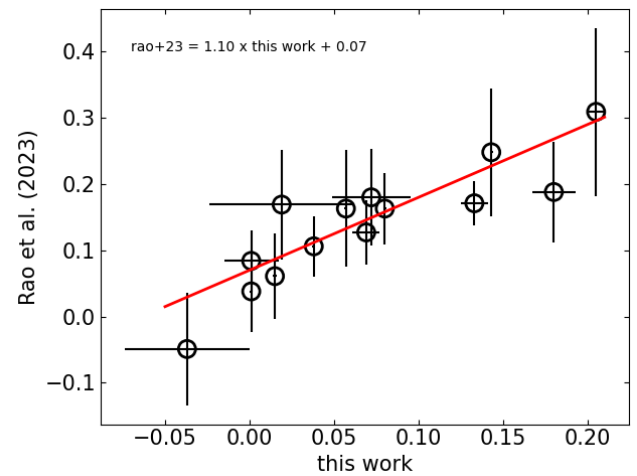


Figure 24. Comparison between A^+ values derived in this work and in Rao *et al.* (2023b).